Catalytic Dehydrogenation on Ultradisperse Sn-Promoted Ir Catalysts Supported on MgAl2O4 Prepared by Different Techniques

Sergio de Miguel, Jayson Fals, Viviana Benitez, Catherine Especel, Florence Epron, Sonia Bocanegra

processes

MDPI

Article

Catalytic Dehydrogenation on Ultradisperse Sn-Promoted Ir Catalysts Supported on $MgAl_2O_4$ Prepared by Different Techniques

Sergio de Miguel [1], Jayson Fals [2], Viviana Benitez [1], Catherine Especel [3], Florence Epron [3] and Sonia Bocanegra [1,*]

[1] Instituto de Investigaciones en Catálisis y Petroquímica (INCAPE)/Consejo Nacional de Investigaciones Científicas y Técnicas (CONICET), Universidad Nacional del Litoral, Santa Fe CP 3000, Argentina; sdmiguel@fiq.unl.edu.ar (S.d.M.); vbenitez@fiq.unl.edu.ar (V.B.)
[2] Grupo de Investigación en Oxi/Hidrotratamiento Catalítico y Nuevos Materiales, Programa de Química-Ciencias Básicas, Universidad del Atlántico, Barranquilla CP 080001, Colombia; jaysonfals@mail.uniatlantico.edu.co
[3] Institut de Chimie des Milieux et Matériaux de Poitiers (IC2MP) CNRS, Université de Poitiers, CP 86000 Poitiers, France; catherine.especel@univ-poitiers.fr (C.E.); florence.epron@univ-poitiers.fr (F.E.)
* Correspondence: sbocane@fiq.unl.edu.ar

Abstract: Ir and IrSn catalysts with different Sn contents (0.5, 0.7 and 0.9 wt%) were prepared using $MgAl_2O_4$ supports synthesized using two different techniques (the citrate–nitrate combustion and coprecipitation methods). Both supports, with a spinel structure, presented low acidity and good textural properties. However, the support prepared by coprecipitation had higher specific surface area and pore volume than the one prepared by combustion, which would favor the dispersion of the metals to be deposited. Likewise, during the preparation of the catalytic materials, a very good interaction was achieved between the metals and both supports, which was confirmed by the presence of sub-nanometer atomic clusters in the mono- and bimetallic catalysts. Regarding the catalytic properties, while the monometallic $Ir/MgAl_2O_4$ samples lead to a very low conversion of n-butane and a selectivity towards hydrogenolysis products, the addition of Sn to Ir increases the conversion, decreases hydrogenolysis and therefore sharply increases the selectivity towards the different butenes. Catalysts with higher Sn loadings present better catalytic behavior. One of the roles of the Sn promoter would be to geometrically modify the Ir clusters, drastically decreasing the hydrogenolytic activity. This effect, added to the strong electronic modification of the Ir sites by the action of Sn, with probable Ir-Sn alloy formation, is responsible for the high catalytic performance of these bimetallic catalysts.

Keywords: $MgAl_2O_4$; IrSn catalysts; dehydrogenation; hydrogenolysis; butenes production

Citation: de Miguel, S.; Fals, J.; Benitez, V.; Especel, C.; Epron, F.; Bocanegra, S. Catalytic Dehydrogenation on Ultradisperse Sn-Promoted Ir Catalysts Supported on $MgAl_2O_4$ Prepared by Different Techniques. *Processes* **2024**, *12*, 1161. https://doi.org/10.3390/pr12061161

Academic Editor: Hsin Chu

Received: 20 May 2024
Revised: 2 June 2024
Accepted: 3 June 2024
Published: 5 June 2024

1. Introduction

In recent years, the global demand for butylenes has grown rapidly, as it plays a fundamental role as a raw material for a wide variety of polymers and products for the chemical industry, such as polybutenes, butylene oxide, sec-butanol, methylethylacetone, acetic acid and maleic anhydride. Normally, butylene is obtained as a by-product from the steam cracking and fluid catalytic cracking of naphtha (FCC). However, due to the increasing demand for butylenes and other light olefins, there is real interest in developing alternative routes for olefin production, in particular from light paraffins frequently found in crude oil-refining plants. The direct dehydrogenation of butane to different butylenes and even diolefin (butadiene) is, therefore, a promising alternative that has already been used industrially in some dehydrogenation processes, such as Oleflex from the UOP company or Catofin from the Houdry company [1–3].

The most common metals used in catalysts for dehydrogenation reactions are Pt or Pd accompanied by metallic promoters such as Sn, In, Ga and Ge [4–10]. Among the noble metals, Ir has been little studied for this type of dehydrogenation reaction. Iridium is a noble metal that has proved to be highly active and selective for syngas production from dry reforming processes, and additionally, it shows a low deactivation by coke [11]. As this metal exhibits high hydrogenolytic activity [12,13], this property can be strongly inhibited by the presence of a metallic promoter [12,14], or by the interaction with particular supports like nanodiamond powders [15]. Considering the properties of high thermal stability, resistance to deactivation by coke and the possibility of inhibiting its hydrogenolytic properties with a promoter metal, Ir seems a good candidate to be studied for the direct dehydrogenation of light paraffins such as n-butane. Indeed, IrSn catalysts, supported on different materials like zeolite and silica, showed good behavior in propane dehydrogenation [12,16,17].

In this paper, the influence of adding different concentrations of a promoter such as Sn to an Ir catalyst with a low metal loading on the dehydrogenating capacity of n-butane is analyzed and the catalytic behaviors are correlated with the surface characteristics of bimetallic catalysts. Likewise, it will be studied if two different synthesis procedures of $MgAl_2O_4$ supports could influence the metal–support interaction and then the catalytic behavior. The impact of the work is based on the fact that, using easily synthesized magnesium aluminate and conventional catalyst preparation techniques that would allow for a simple scale-up at an industrial level, ultradisperse supported IrSn catalysts with very good catalytic performance in the n-butane dehydrogenation are developed.

2. Materials and Methods

For the synthesis of $MgAl_2O_4$ using the citrate–nitrate combustion method ($MgAl_2O_4$-citr), a solution was prepared with citric acid ($C_6H_8O_7 \cdot H_2O$), magnesium nitrate, $Mg(NO_3)_2 \cdot 6H_2O$, aluminum nitrate, $Al(NO_3)_3 \cdot 9H_2O$ at a molar ratio of citric acid/NO_3^- ions equal to 0.5 and Al/Mg at a molar ratio equal to 2. Then, the mixture was brought to a boil for 30 min with mild stirring, achieving the formation of a yellowish gel. The gel was dried in a vacuum oven for 1 h at 75 °C and then for 23 h at 100 °C. Then, the dry gel underwent a complex calcination process in a N_2 flow, then in a N_2(95%)/O_2(5%) mixture and finally in air at 800 °C. The citric acid/nitrate ion ratio was always kept constant in all experiments by the precise determination of the concentrations of the citric acid (by titration with the NaOH solution), aluminum nitrate and magnesium nitrate solutions (by ICP), and the careful measurement of the volumes in the mixtures. For more details about this method see reference [18].

For the synthesis of the $MgAl_2O_4$ by the coprecipitation method with $(NH_4)_2CO_3$ ($MgAl_2O_4$-cop), a solution was prepared with magnesium nitrate, $Mg(NO_3)_2 \cdot 6H_2O$, aluminum nitrate and $Al(NO_3)_3.9H_2O$ at a molar ratio of Al/Mg equal to 2. A solution of ammonium carbonate, 1 mol L^{-1} $(NH_4)_2CO_3$, with twice the volume of the solution of Al and Mg nitrates, was prepared separately. The ammonium carbonate solution was placed under vigorous stirring and the Al and Mg nitrate solution was added at a flow rate of 120 mL/h using a peristaltic pump at room temperature. A gel was formed that was left to mature for 12 h and then filtered. The gel was washed with distilled water in the following way: the gel was placed in a beaker and its volume was increased 6 times with water, left to stir vigorously for 20 min and filtered again. The gel was dried in an oven at 100 °C for 12 h and ground in a ceramic mortar, forming a fine powder. Finally, it was placed in a quartz reactor and calcined in an air flow of 100 mL/min for 3 h at 800 °C to form the spinel.

The Ir and IrSn catalysts were prepared by incipient impregnation at room temperature. For the iridium catalysts, a solution of $H_2IrCl_6 \cdot 6H_2O$ was used as precursor. This solution had an adequate concentration to achieve 0.5 wt% of Ir content in the monometallic samples. The impregnated supports were dried in an oven at 100 °C for 12 h and then calcined in an air flow at 500 °C for 3 h. For the bimetallic IrSn catalysts, once the Ir was impregnated onto the supports, they were dried in an oven at 100 °C for 12 h. Then, they were impregnated

with a $SnCl_2$ precursor solution with concentrations such as to achieve Sn contents of 0.5, 0.7 and 0.9 wt%. The impregnated supports were dried in an oven at 100 °C for 12 h and then calcined in an air flow at 500 °C for 3 h.

XRD measurements for precursor and calcined supports were performed on an Empyrean PANALYTICAL diffractometer with a copper anode (λ = 1.54060 Å). The measurement conditions were: 40 kV and 40 mA with a step size of 0.01° (in 2θ) and a scan step time of 0.6 s.

The specific surface and both the pore volume and pore size distribution for the different types of $MgAl_2O_4$ were obtained using the BET and BJH methods from nitrogen adsorption isotherms at −196 °C in a Micromeritics (Norcross, GA, USA) static volumetric instrument, model ASAP 2020, after degassing the samples in a high vacuum.

The acidic properties (Brönsted and Lewis acid sites ratio) of the supports were evaluated by means of diffuse reflectance infrared Fourier transform spectroscopy of pyridine (DRIFTS-Py) in a Shimadzu FTIR, Affinity-1S (Kyoto, Japan). The weight (25 mg) of each sample was heated in situ in the cell for 30 min under vacuum at 400 °C. The cell was cooled to 150 °C and the background spectrum was recorded. Nitrogen saturated with Pyridine at atmospheric pressure was then introduced into the cell at 150 °C for 30 min. All measurements were performed at this temperature to prevent the physisorption of pyridine. The sample was then heated for 30 min at 200 °C, cooled down to 150 °C, and the spectrum was recorded by averaging 64 scans with a resolution of 4 cm^{-1}.

TPR experiments were carried out by heating the samples from room temperature up to 650 °C at a heating rate of 6 °C min^{-1}. The reducing mixture H_2 (5% v/v)/N_2 was fed to the reactor at a flow rate of 9 mL min^{-1}. The catalysts were previously calcined in air at 500 °C for 2 h.

XPS measurements were performed on a Multitechnique Specs instrument equipped with a dual Mg/Al X-ray source model XR50 and a PHOIBOS 150 hemispherical analyzer in fixed analyzer transmission (FAT) mode. The spectra were obtained with a pass energy of 30 eV and an Al anode operated at 100 W. The samples were supported on double-sided Cu tape and subjected to evacuation in an ultra-high vacuum prior to the measurements ($2 \cdot 10^{-8}$ mbar). Additionally, the samples were pre-reduced at 530 °C for 2 h.

TEM measurements were carried out in a JEOL transmission electron microscope, model JEM-2100 Plus, using an accelerating voltage of 200 kV. The samples were dispersed with ethanol or acetone in an ultrasound bath, and deposited on a 300 mesh copper grid covered with Lacey Carbon film. To carry out the size distribution of the metal particles, a very important number of particles (>100) was measured. The formula to calculate the mean metallic particle diameter (D) was $D = \Sigma i\ ni.\ di/\Sigma i\ ni$, where ni is the number of particles with diameter di.

The cyclopentane hydrogenolysis (reaction test for the metallic phase) was carried out in a differential flow reactor using a volumetric flow of 6 mL·h^{-1}. Prior to the reactions, the catalysts were reduced in situ under a H_2 flow for 2 h at 500 °C and the reaction products were analyzed by gas chromatography. The reaction was carried out at 500 °C using a H_2/cyclopentane molar ratio equal to 22.

The catalysts were evaluated in the n-butane dehydrogenation reaction, carried out in a continuous flow reactor at 530 °C for 2 h. The reactor (with a catalyst weight of 0.200 g) was fed with 18 mL min^{-1} of the reaction mixture (n-butane + hydrogen, molar ratio H_2/n-C_4H_{10} = 1.25). Before the reaction, the catalysts were reduced in situ at 530 °C under a flow (100 mL min^{-1}) of H_2 for 2 h. The reactor effluent was analyzed with a gas chromatograph with an FID detector and a packed column, determining the different reaction products (1-butene, cis-2-butene, trans-2-butene, 1,3-butadiene, propane, propylene, ethane, ethylene and methane), in addition to the unconverted reactant (n-butane). The n-butane conversion was calculated on the basis of the sum of the values of the chromatographic areas of the reaction products (corrected by the corresponding response factors and its molecular weight) relative to the n-butane fed to the reactor. The selectivity to all butenes was calculated as the ratio between the moles of total butenes (1-butene, cis- and trans-2-butene

and butadiene) with respect to the moles of all reaction products (except for H_2). The loss of conversion (ΔX) was calculated as: $((X_{initial} - X_{final})/X_{initial}) \times 100$. The yield (Y) towards total butenes was defined as the product between the n-butane conversion and the selectivity to butenes.

In the case of the carbon balance, the flow rates of the feed and product streams were measured using a precision flowmeter. The chromatographic peak areas of the carbon-containing molecules were used to achieve a C balance between the input and output streams. This balance showed an error of approximately 3%, which was considered an acceptable value. Furthermore, no carbon imbalance could be detected due to coke deposition on the catalytic surface or on the reactor walls.

3. Results

3.1. Characterization of the Supports

Regarding the $MgAl_2O_4$-citr synthesis, X-ray diffraction analysis was carried out to determine the $MgAl_2O_4$ formation. The diffractogram displayed in Figure 1 shows all the peaks corresponding to the magnesium aluminate spinel.

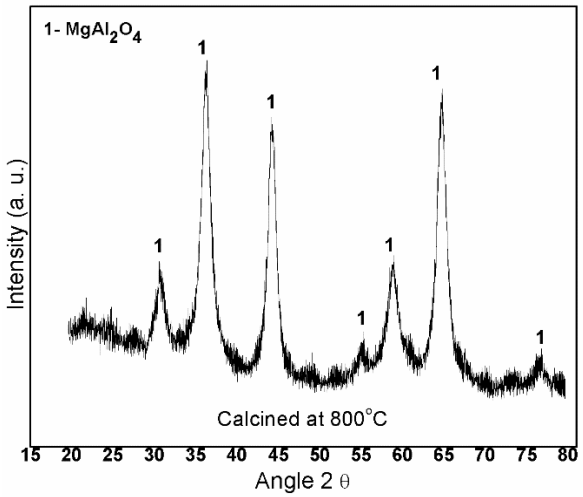

Figure 1. XRD diffractogram of the $MgAl_2O_4$-citr support after the calcination at 800 °C.

Regarding the coprecipitation synthesis, the objective of this technique using ammonium carbonate as a precipitating agent is to obtain the formation of precursor compounds (Mg/Al double hydroxides or hydrotalcite), which can lead to magnesium aluminate spinel after decomposition [19,20] with improved textural properties such as higher surface area and pore volume, than the combustion method. Figure 2 shows XRD results that correspond to the synthesis of $MgAl_2O_4$-cop. In the XRD profile of the precursor, it is seen that the coprecipitation of nitrates originates a precursor whose main phase is hydrotalcite, $MgAl_2(CO_3)(OH)_{16}{\cdot}4H_2O$, with a stoichiometric Mg/Al ratio equal to that of magnesium aluminate. As mentioned before, this compound can produce $MgAl_2O_4$ by thermal decomposition. After the calcination of the coprecipitated precursor, the formation of the magnesium aluminate was confirmed.

The textural properties of both $MgAl_2O_4$ supports were characterized by N_2 physisorption. The results are presented in Table 1. Figures 3 and 4 show the pore size distributions for both materials. According to the International Union of Pure and Applied Chemistry (IUPAC), porous materials are classified into three types according to the size of the pores: microporous (a pore size < 2 nm), mesoporous (a pore size between 2 and 50 nm) and macroporous (a pore size > 50 nm).

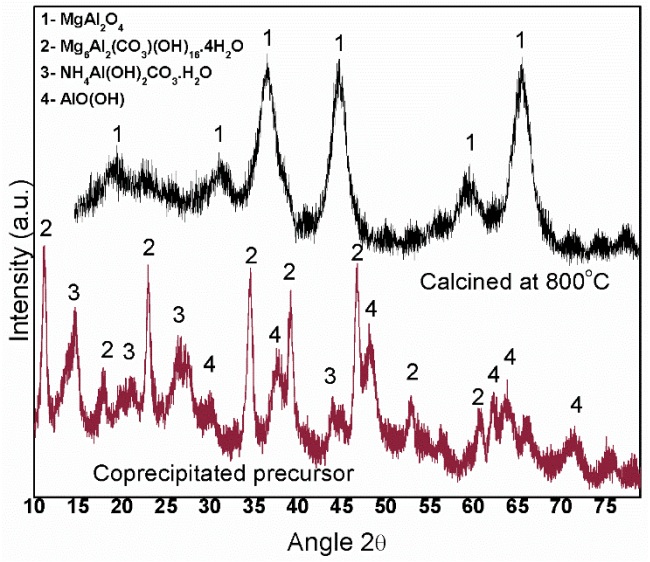

Figure 2. XRD diffractograms of the precursor obtained by the coprecipitation method and after the calcination at 800 °C.

Table 1. Textural properties of both $MgAl_2O_4$ supports.

Property	$MgAl_2O_4$-citr	$MgAl_2O_4$-cop
Specific surface (S_{BET})	129 m^2 g^{-1}	191 m^2 g^{-1}
Pore volume	0.089 cm^3 g^{-1}	0.801 cm^3 g^{-1}
Average pore diameter	28 Å	168 Å

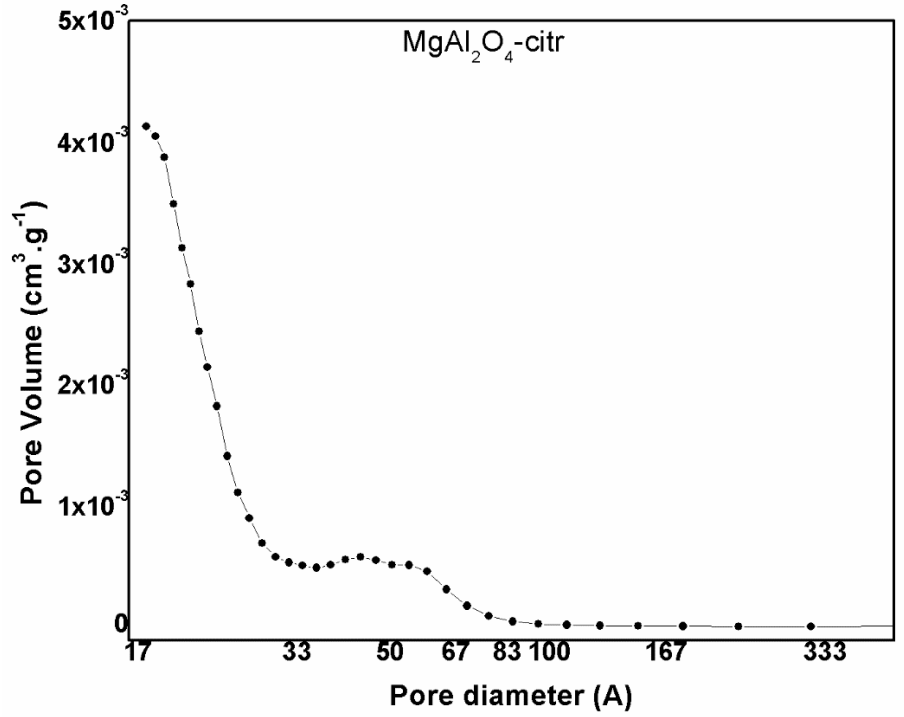

Figure 3. Pore size distribution for $MgAl_2O_4$-citr.

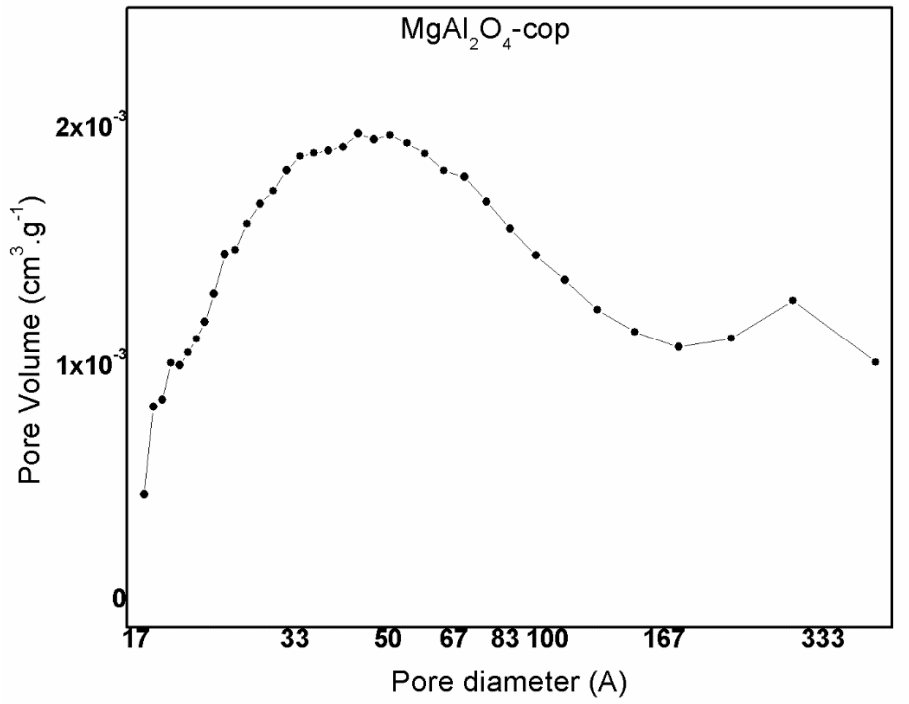

Figure 4. Pore size distribution for $MgAl_2O_4$-cop.

In Figure 3, it can be seen that the synthesis of $MgAl_2O_4$ using the citrate–nitrate combustion method ($MgAl_2O_4$-citr) led to a material with both very small pores (micropores < 20 Å) and pores of a larger size (mesopores and macropores between 20 and 100 Å). In this sense, this material displays mainly a mixture of micro- and mesoporosity. On the other hand, Figure 4 shows that the preparation of $MgAl_2O_4$ by the coprecipitation method ($MgAl_2O_4$-cop) led to a material that is essentially mesoporous, with a broad and main zone that corresponds to a pore size distribution between 20 and 200 Å and a second and small distribution peak between 200 and 400 Å. In this material, there is a small fraction of micropores with diameters < 20 Å.

From the comparison of the physical properties of both supports (Table 1), it is observed that the $MgAl_2O_4$ prepared by coprecipitation has a higher specific surface area and a much higher pore volume than that synthesized using the citrate–nitrate combustion method.

Figure 5 shows DRIFTS spectra of the pyridine adsorbed on both supports. This analysis was carried out for determining the acidity of the materials (type of acid sites). It must be noted that the Bronsted acid sites are located between 1530 and 1560 cm^{-1} and the Lewis sites between 1440 and 1470 cm^{-1} [21]. For comparison purposes, the spectrum corresponding to a low acidity γ-alumina is added, which presents a higher development of Bronsted and Lewis acidity. As can be seen in Figure 5, both the $MgAl_2O_4$-cop and $MgAl_2O_4$-citr supports do not present Bronsted acid sites, but the $MgAl_2O_4$-cop presents Lewis acid sites in a low concentration. These results indicate the low acidity of both supports, though the support obtained by coprecipitation is a little more acidic than that obtained using the citrate–nitrate method.

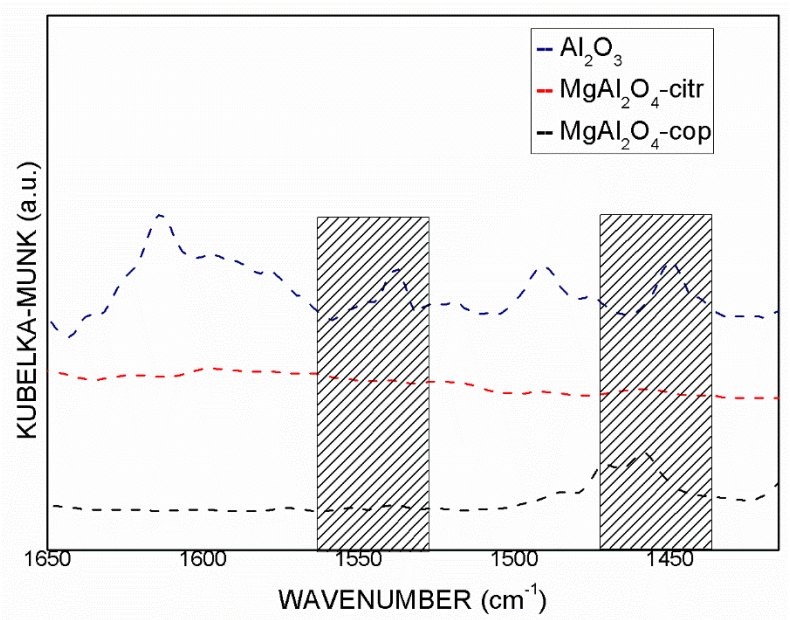

Figure 5. DRIFTS-Py analysis of the $MgAl_2O_4$-cop and $MgAl_2O_4$-citr supports.

3.2. Catalytic Evaluation

Figures 6 and 7 show the activity results of n-butane dehydrogenation reaction for mono Ir and bimetallic IrSn catalysts supported on $MgAl_2O_4$-citr and $MgAl_2O_4$-cop, respectively. Concerning the monometallic Ir catalysts, there are differences between the catalytic behavior of both samples. While the catalyst Ir(0.5)/$MgAl_2O_4$-citr presented an initial conversion ($X_{initial}$) of 22% and a loss of activity of 49% over the 2 h reaction time (Figure 6 and Table 2), the Ir(0.5)/$MgAl_2O_4$-cop catalyst had a higher initial conversion (26%) and a lower drop of activity (36%) (Figure 7 and Table 2).

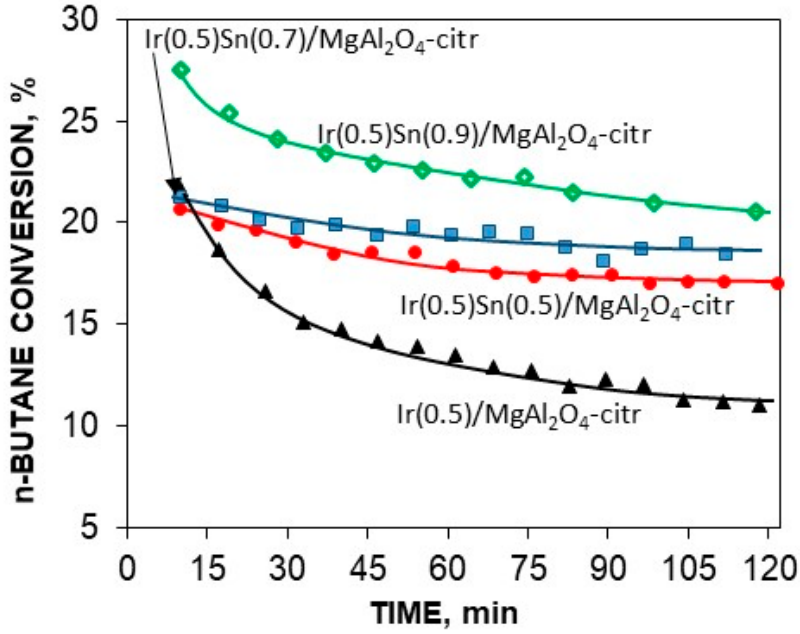

Figure 6. N-butane conversion vs. reaction time for Ir and IrSn catalysts supported on $MgAl_2O_4$-citr.

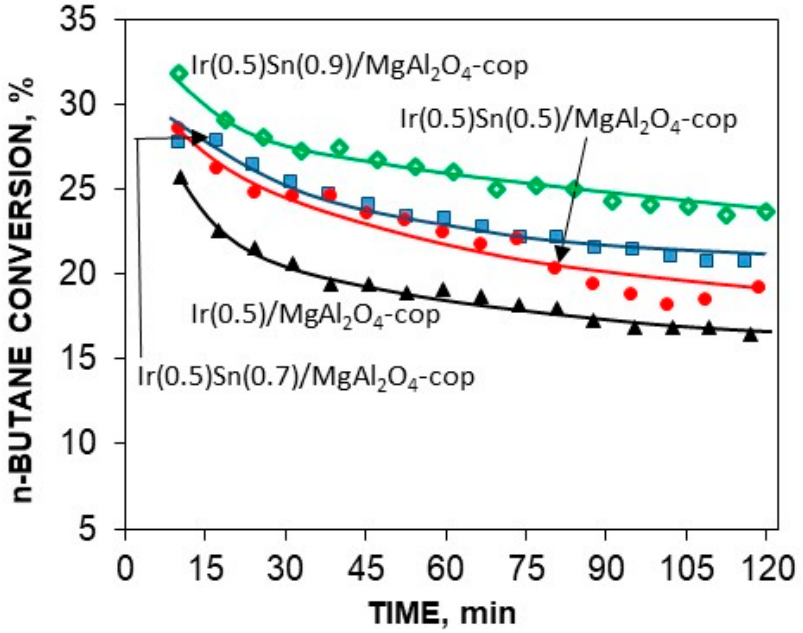

Figure 7. N-butane conversion vs. reaction time for Ir and IrSn catalysts supported on $MgAl_2O_4$-cop.

Table 2. Results of n-butane dehydrogenation. X_0: initial conversion; X_f: final conversion; ΔX: $((X_0 - X_f)/X_0) \times 100$ (loss of conversion); S_0: initial selectivity to total butenes; S_f: final selectivity to total butenes; Y_0: initial yield to butenes; Y_f: final yield to butenes.

Catalyst	X_0 (%)	X_f (%)	ΔX (%)	S_0 (%)	S_f (%)	Y_0 (%)	Y_f (%)
Ir(0.5)-$MgAl_2O_4$-cop	26	17	36	20	25	5	4
Ir(0.5)-$MgAl_2O_4$-citr	22	11	49	22	26	5	3
Ir(0.5)Sn(0.5)-$MgAl_2O_4$-cop	29	19	33	60	81	17	16
Ir(0.5)Sn(0.5)-$MgAl_2O_4$-citr	21	17	17	72	84	15	14
Ir(0.5)Sn(0.7)-$MgAl_2O_4$-cop	28	21	25	71	85	20	18
Ir(0.5)Sn(0.7)-$MgAl_2O_4$-citr	21	18	15	80	90	17	16
Ir(0.5)Sn(0.9)-$MgAl_2O_4$-cop	32	24	25	65	84	21	20
Ir(0.5)Sn(0.9)-$MgAl_2O_4$-citr	28	21	24	66	86	18	17

The addition of tin to the monometallic catalyst did not strongly change the values of the initial conversion but improved the stability, since the conversion loss was less significant, and this gain in stability increased with the content of tin. As for the monometallic catalysts, there was an effect of the support. The bimetallic IrSn catalysts supported on $MgAl_2O_4$-citr showed lower initial conversions and a lower conversion loss than those supported on $MgAl_2O_4$-cop, whatever the tin content. For the $MgAl_2O_4$-cop support, the initial and final conversions (see Table 2) of the bimetallic catalysts did not vary strongly with the tin content with values of initial conversion (X_0) between 28 and 32%, and final conversions (X_f) in the range of 19–24%. The loss of conversion was lower in the catalysts with higher Sn contents (25%). Considering the bimetallic catalysts supported on $MgAl_2O_4$-citr, the initial conversions for Ir(0.5)Sn(0.5)/$MgAl_2O_4$-citr and Ir(0.5)Sn(0.7)/$MgAl_2O_4$-citr were similar to that of the corresponding monometallic sample, at about 21% (see Table 2), but the Ir(0.5)Sn(0.9)/$MgAl_2O_4$-citr catalyst had a higher X_0 value (28%). The activity loss for the bimetallic catalysts supported on $MgAl_2O_4$-citr was low and ranged from 15 to 24% (Table 2).

With respect to the total selectivity to butenes (Figures 8 and 9 and Table 2), there was a very marked difference between the monometallic and bimetallic catalysts. The

monometallic samples showed very low selectivity to butenes (between 20 and 26%), while the bimetallic ones had values ranging between 60 and 90%.

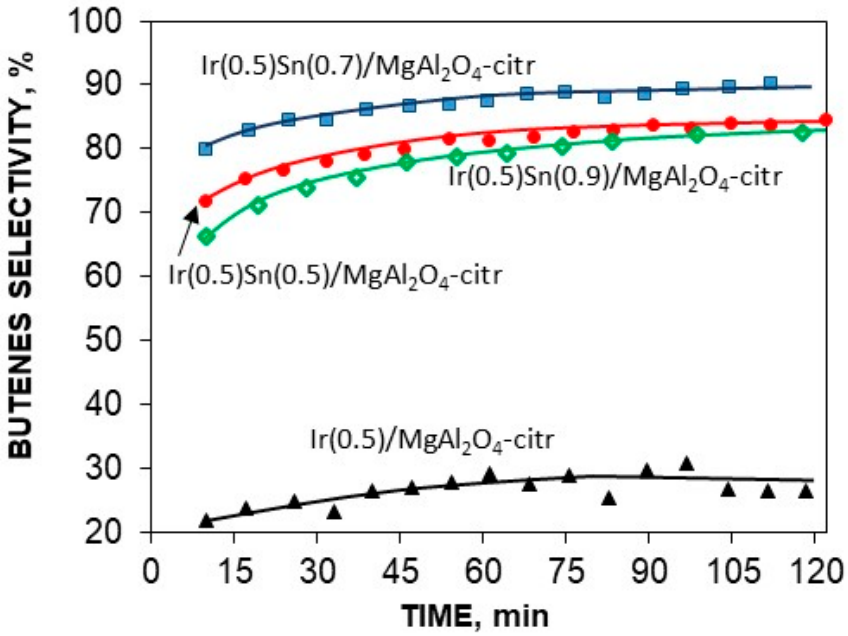

Figure 8. Selectivities to total butenes as a function of the reaction time for Ir and IrSn supported on $MgAl_2O_4$ prepared using the citrate–nitrate method.

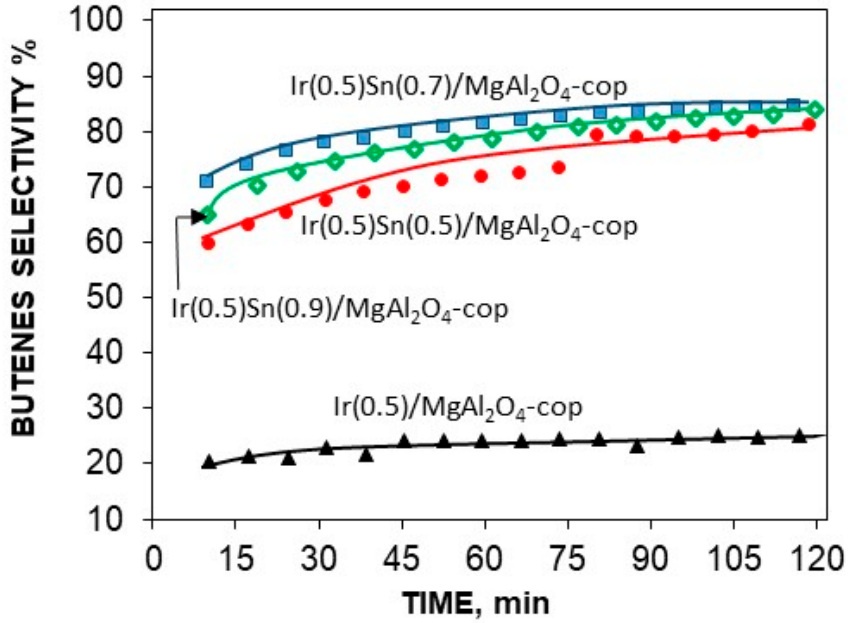

Figure 9. Selectivities to total butenes as a function of the reaction time for Ir and IrSn supported on $MgAl_2O_4$ prepared by coprecipitation.

Both types of bimetallic catalysts increase their selectivity values (Figures 8 and 9) with the increase of the Sn content. At the end of the reaction time, the selectivities to butenes reached values between 81 and 85% for the bimetallic catalysts supported on $MgAl_2O_4$-cop (see Figure 9 and Table 2), while for the corresponding bimetallic catalysts supported on $MgAl_2O_4$-citr, the final selectivities were higher, in the range of 84–90% (see Figure 8 and Table 2).

The yield to butenes (Y) as a function of the reaction time is shown in Figures 10 and 11 and Table 2. This parameter is important at an industrial level, since it measures the total moles of olefins produced per mol of n-butane in the feed. It can be observed that both monometallic catalysts presented low yield values of about 3–5%. The addition of Sn to Ir produced a notable improvement in butene yields, reaching maximum values of 18% for the Ir(0.5)Sn(0.9)/$MgAl_2O_4$-citr catalyst and 21% for the bimetallic counterpart supported on coprecipitated $MgAl_2O_4$ (Table 2). In conclusion, both series of catalysts presented good catalytic behavior, with the bimetallic ones supported on coprecipitated $MgAl_2O_4$ being slightly better.

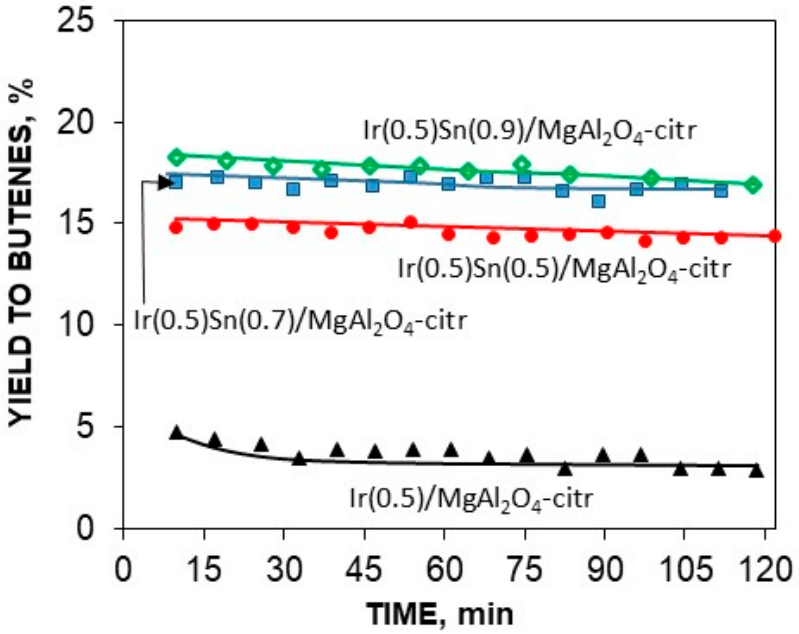

Figure 10. Yield to total butenes as a function of the reaction time for Ir and IrSn supported on $MgAl_2O_4$ prepared using the citrate–nitrate method.

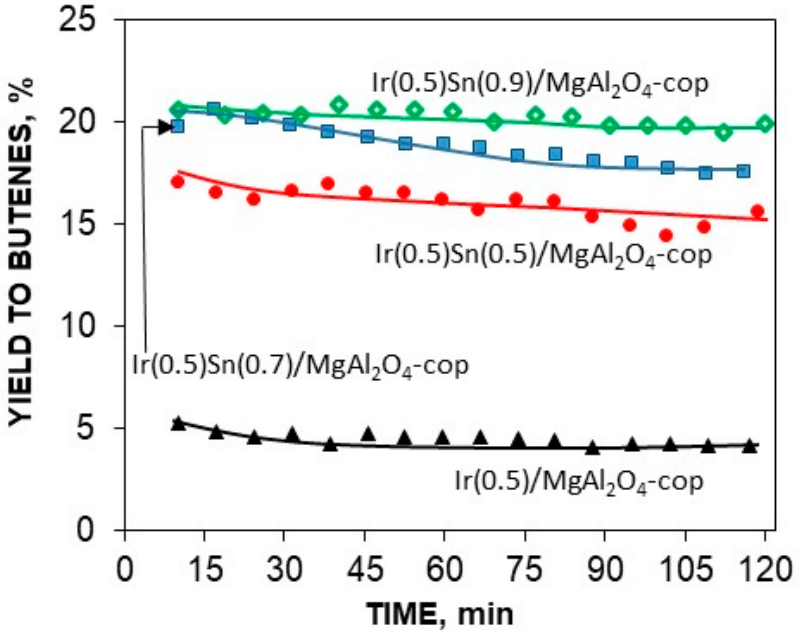

Figure 11. Yield to total butenes as a function of the reaction time for Ir and IrSn supported on $MgAl_2O_4$ prepared by coprecipitation.

With respect to the coke deposition during the reaction, temperature programmed oxidation (TPO) experiments showed that the carbon contents of bimetallic catalysts were negligible (less than 0.1 wt%).

With respect to the influence of Sn on the catalytic behavior of IrSn catalysts, a significant increase in selectivity to butenes was observed as the amount of this metal promoter in the samples increased. However, this is true for Sn contents of 0.5 and 0.7 wt%, but when 0.9 wt% of Sn was added to the Ir catalyst, the selectivity did not improve compared to the catalyst with 0.7 wt% of Sn.

If the influence of the support synthesis method on the catalytic behavior is analyzed, it can be concluded that the catalysts supported on $MgAl_2O_4$-cop are more active, but less selective than those supported on $MgAl_2O_4$-citr. However, the higher selectivity to butenes of the catalysts supported on $MgAl_2O_4$-citr does not compensate for the higher activity of the catalysts supported on $MgAl_2O_4$-cop, and therefore the yield to butenes is slightly higher in the latter catalysts.

In the n-butane dehydrogenation process, the dehydrogenation reactions lead to butenes (1-butene, cis- and trans-2-butene, and butadiene), but undesired hydrogenolysis reactions also take place, that is, the breaking of C-C bonds generating C1-C3 light products, and the formation reaction of coke via Diels–Alder addition and the condensation of butadiene with butenes or other products [22]. Butenes isomerization to isobutenes is catalyzed by strong acidic catalysts by strong acidic catalysts [23], but this cannot occur in non-acidic supports like magnesium spinels. Without considering the coke formation, basically what is not dehydrogenating selectivity is selectivity towards hydrogenolysis products, and then the selectivity towards hydrogenolysis in percentages can be determined by the difference between 100 and the selectivity towards dehydrogenation. Therefore, from Table 2, the selectivity towards hydrogenolysis products can be determined, and it is very high for monometallic Ir catalysts (between 75 and 80%), while as Sn is added to Ir, a drastic decrease of hydrogenolysis reactions occurs, reaching final hydrogenolysis selectivity values lower than 20%.

To better understand what happens to the hydrogenolytic behavior of the catalysts, they were evaluated in a typical test reaction, the cyclopentane hydrogenolysis (CPH). The rupture of the cyclopentane ring gives rise to the formation of n-pentane, but if the hydrogenolysis is deeper, the rupture of other C-C bonds occurs, giving rise to the formation of C4, C3 and C2 compounds, in addition to methane. This hydrogenolysis reaction, as also happens with the n-butane hydrogenolysis, is structure-sensitive and requires an ensemble of metal atoms [24–26]. Table 3 shows initial reaction rate values in the CPH reaction for the different catalysts (R^o_{CP}), which show a very high hydrogenolytic activity for both monometallic Ir catalysts. Both monometallic samples displayed high percentages of light products (C1–C4) and low amounts of n-pentane (Table 3). It can be seen that Ir alone has an important capacity to break cyclic compounds and C-C bonds [27–29]. Ir atomic ensembles are able to adequately adsorb the CP molecule and produce the C-C breaks in all parts, giving mainly methane and another light gases, while the selectivity to n-pentane is very low (<3%) in both Ir catalysts. The Sn addition to Ir on both supports produces an important decrease in the CP hydrogenolytic capacity of the catalysts, this effect being more pronounced with bimetallic catalysts supported on coprecipitated $MgAl_2O_4$. In this sense, the drop in the hydrogenolysis reaction rate (R^o_{CP}) for the bimetallic catalyst with the highest Sn content (0.9 wt%) with respect to the corresponding monometallic catalyst was 49 times for the sample supported on $MgAl_2O_4$-cop and 23 times for that supported on $MgAl_2O_4$-citr, which shows the strong decrease of the hydrogenolytic capacity due to the effect of the metallic promoter. As CPH is a reaction sensitive to the structure that requires the adsorption of the reactant on an ensemble of atoms, the function of Sn would be to intercalate between the atoms of the active metal (Ir), breaking the ensemble and therefore drastically decreasing the hydrogenolytic capacity, and/or to electronically modify the active metal. These CP hydrogenolysis results clearly explain the very good catalytic behavior in butane dehydrogenation of these bimetallic catalysts due to the beneficial

action of Sn on Ir, inhibiting the strong hydrogenolytic behavior of the active metal and hence increasing the dehydrogenation selectivity towards butenes.

Table 3. Results of CP hydrogenolysis. R^0_{CP}: initial reaction rate of CPH. S: selectivity.

Catalysts	S to Light Products (%)	S to n-pentane (%)	R°_{CP} (mol h^{-1} $gcat^{-1}$)
Ir(0.5)/$MgAl_2O_4$ citr	97.4	2.6	96.1
Ir(0.5)Sn(0.5)/$MgAl_2O_4$ citr	22.6	77.4	9.6
Ir(0.5)Sn(0.7)/$MgAl_2O_4$ citr	15.2	84.8	7.5
Ir(0.5)Sn(0.9)/$MgAl_2O_4$ citr	8.8	91.2	4.1
Ir(0.5)/$MgAl_2O_4$-cop	99.9	0.1	185.1
Ir(0.5)Sn(0.5)$MgAl_2O_4$-cop	18.3	81.7	5.7
Ir(0.5)Sn(0.7)/$MgAl_2O_4$-cop	49.4	50.6	4.7
Ir(0.5)Sn(0.9)/$MgAl_2O_4$-cop	66.7	33.3	3.8

When comparing these results with those of the n-butane dehydrogenation reaction, it can be observed that the catalysts supported on $MgAl_2O_4$-cop always had a hydrogenolytic selectivity that was somewhat higher than the corresponding ones supported on $MgAl_2O_4$-citr. Correspondingly, in CPH, the Ir(0.5)/$MgAl_2O_4$-cop catalyst had twice the R^o_{CP} value of the Ir(0.5)/$MgAl_2O_4$-citr catalyst. However, with the addition of Sn, the bimetallic catalysts supported on $MgAl_2O_4$-citr displayed a gradual decrease in hydrogenolytic activity (Table 3), while the bimetallic catalysts supported on $MgAl_2O_4$-cop showed a sharp drop in the R^o_{CP} value with respect to that of the monometallic one with the first addition of Sn (0.5 wt%), and then there was a small decrease with the increase of the Sn content (Table 3). With respect to the deeper CP hydrogenolytic selectivity, concerning the multiple breaking of C-C bonds that leads to light gases, this selectivity to light compounds was drastically decreased by the addition of Sn to Ir in both series of catalysts, mainly in those supported on $MgAl_2O_4$-citr (see Table 3). These facts reveal that the structure of the Ir metallic particles supported on $MgAl_2O_4$-citr is different from that supported on $MgAl_2O_4$-cop, and that the addition of Sn influences both in different ways.

3.3. Characterization of Catalysts

The catalysts were characterized by TPR, XPS and TEM in order to correlate the catalytic behavior with the metallic phase properties. Temperature-programmed reduction (TPR) experiments were performed to determine and evaluate the reducibility of the metallic species (Figures 12 and 13). The TPR profile of the Ir/$MgAl_2O_4$-citr displays a hydrogen consumption peak centered at 260 °C (Figure 12), while for the Ir/$MgAl_2O_4$-cop catalyst the peak is located at 240 °C (Figure 13). These peaks can be ascribed to the complete reduction of IrO_2 to metallic Ir. Similar TPR results were obtained for Ir catalysts supported on KIT-6 (an ordered mesoporous silica with a cubic arrangement of interconnected pores) and supported on doped alumina [11,30].

The TPR profiles of the IrSn/$MgAl_2O_4$-citr catalysts (Figure 12) are very similar to the corresponding signals of IrSn/$MgAl_2O_4$-cop (Figure 13). They show a main reduction peak located at temperatures close to those corresponding to the monometallic Ir sample (between 240 °C and 270 °C), and an additional important reduction area between 350 and 580 °C. The main peaks are wider than those of the corresponding monometallic catalyst and would be due to a co-reduction of Ir and Sn oxides (a possible spillover effect) or to the formation of alloyed Ir-Sn species, since these peaks have a higher area with respect to that observed in the corresponding monometallic catalysts. These facts would indicate the presence of important interactions between iridium and tin with probable alloy formation. This effect would be more pronounced for both types of bimetallic catalysts with the highest

Sn loading (0.9 wt%) since a shift to lower reduction temperatures of the main reduction peak is observed. The reduction zone at high temperatures (between 350 and 580 °C) observed in Figures 12 and 13 can be attributed to the reduction of oxidized species of Sn in strong interaction with the support, with similar results being found for PtSn catalysts supported on $MgAl_2O_4$ [18].

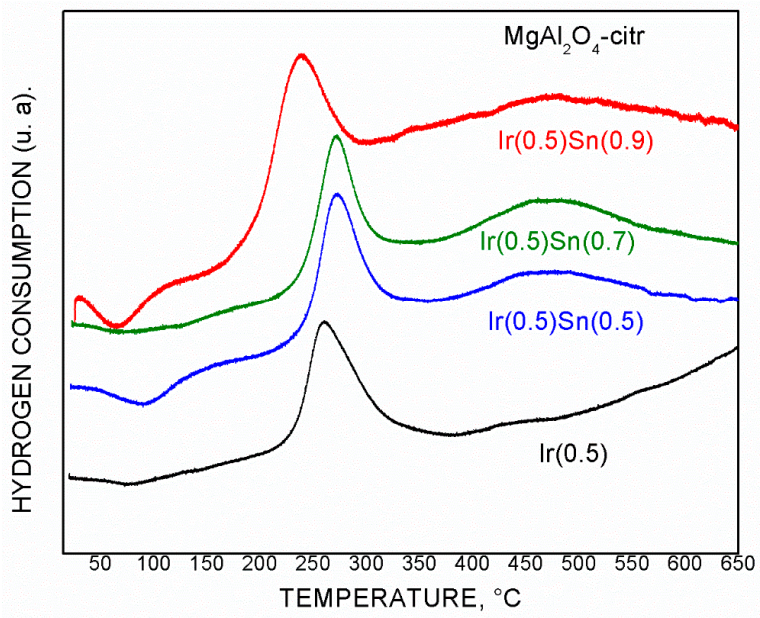

Figure 12. TPR profiles of Ir and IrSn catalysts supported on $MgAl_2O_4$-citr.

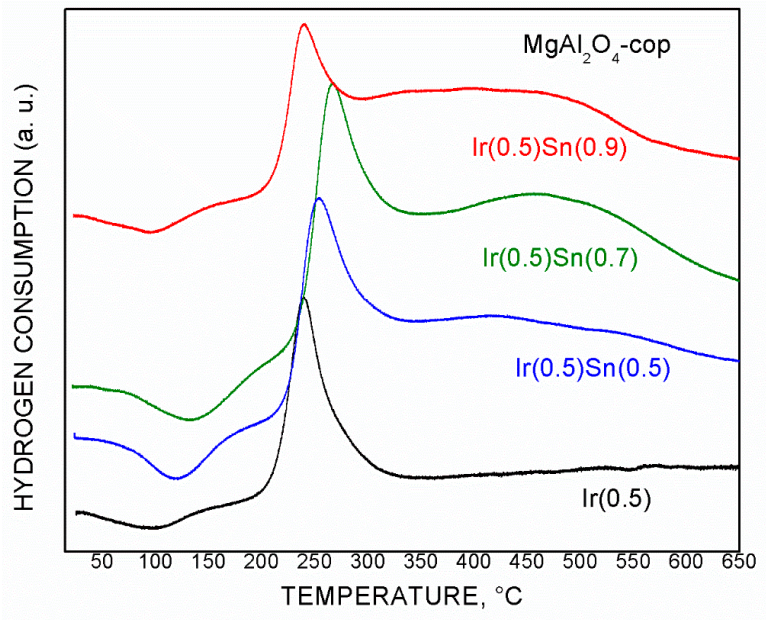

Figure 13. TPR profiles of Ir and IrSn catalysts supported on $MgAl_2O_4$-cop.

Selected bimetallic and monometallic catalysts were chosen to determine particle size distributions by TEM and to analyze the possible size modifications after the addition of Sn to Ir. Figures 14 and 15 show the histograms of particle size distribution for the monometallic Ir(0.5)/$MgAl_2O_4$-citr and the bimetallic Ir(0.5)Sn(0.7)/$MgAl_2O_4$-citr, and for the monometallic Ir (0.5)/$MgAl_2O_4$-cop and the bimetallic Ir(0.5)Sn(0.7)/$MgAl_2O_4$-cop, respectively. Figure 16 shows the corresponding TEM images for the different catalysts. The most relevant fact is that the catalysts display very low particle sizes, of less than

0.8 nm, which means that they have an ultradisperse metallic phase. It must be remarked that the fraction of surface sites increases as the size of metallic particles decreases. Some authors [31,32] have confirmed that a change occurs in the electronic structure of metallic particles at a critical diameter of 2 nm, where at sizes larger than 2 nm there would be nanoparticles and at sizes lower than 2 nm, clusters of atoms. Therefore, these ultradisperse mono- and bimetallic catalysts are constituted as atomic clusters [15].

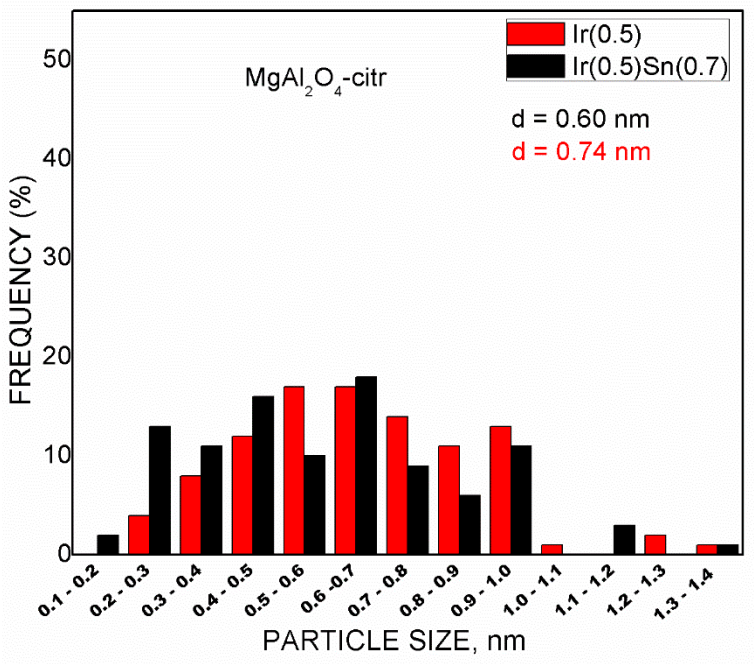

Figure 14. Histograms of particle size distribution for Ir(0.5)/$MgAl_2O_4$-citr and Ir(0.5)Sn(0.7)/$MgAl_2O_4$-citr catalysts. d = average particle sizes (nm).

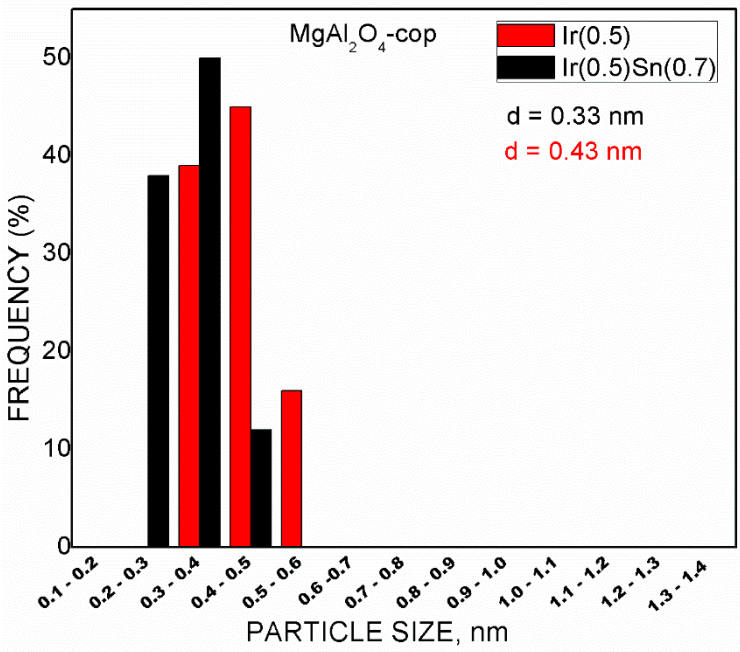

Figure 15. Histograms of particle size distribution for Ir(0.5)/$MgAl_2O_4$-cop and Ir(0.5)Sn(0.7)/$MgAl_2O_4$-cop catalysts. d = average particle sizes (nm).

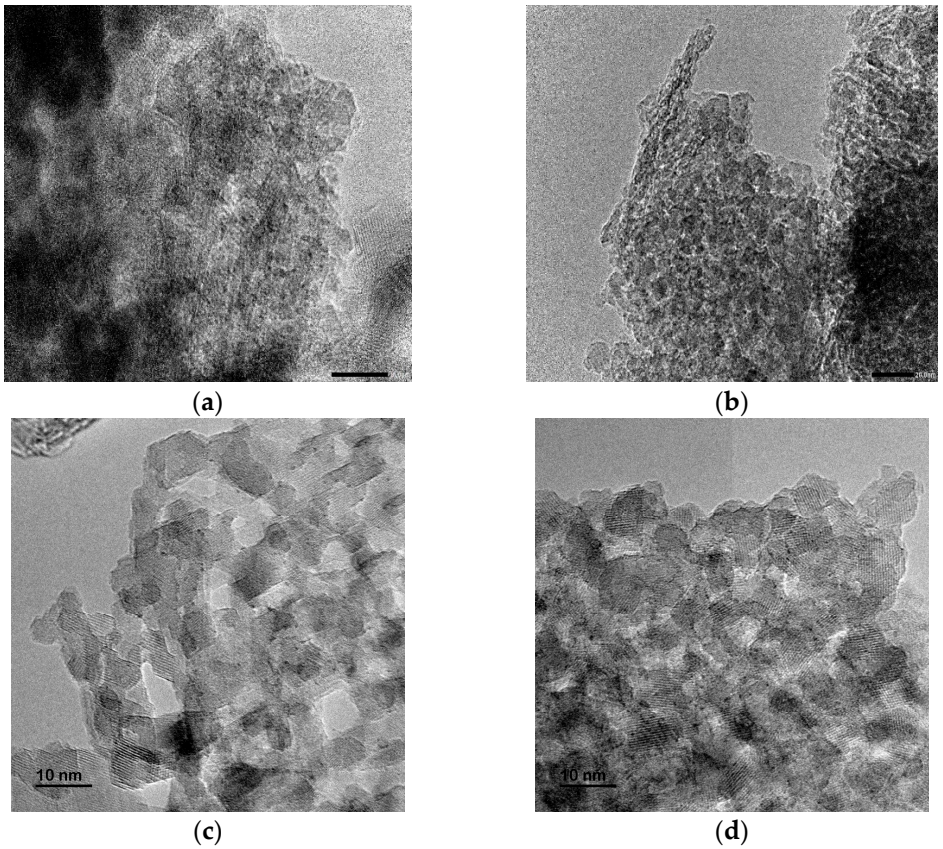

Figure 16. TEM images of (**a**) Ir(0.5)/$MgAl_2O_4$-citr, (**b**) Ir(0.5)Sn(0.7)/$MgAl_2O_4$-citr, (**c**) Ir(0.5)/$MgAl_2O_4$-cop and (**d**) Ir(0.5)Sn(0.7)/$MgAl_2O_4$-cop.

The size distribution of the clusters of both catalyst series is different. While the Ir and IrSn catalysts supported on $MgAl_2O_4$ obtained using the citrate–nitrate method present a wide distribution ranging from sizes of 0.2 to 1.4 nm (Figure 14), the mono- and bimetallic samples supported on $MgAl_2O_4$ synthesized by coprecipitation show a very narrow distribution, between 0.2 and 0.6 nm (Figure 15). If we compare the average particle diameters, the catalysts supported on $MgAl_2O_4$-cop have smaller sizes than those supported on $MgAl_2O_4$-citr. Furthermore, it should be mentioned that in both series, the bimetallic catalysts presented slightly smaller average sizes than the corresponding monometallic ones, decreasing from 0.74 to 0.60 nm for the catalysts supported on $MgAl_2O_4$-citr and from 0.43 to 0.33 nm for those supported on $MgAl_2O_4$-cop.

Figures 17 and 18 show the XPS spectra of the Ir $4f_{7/2}$ and Ir $4f_{5/2}$ signals for both reduced monometallic catalysts, Ir(0.5)/$MgAl_2O_4$-citr and Ir(0.5)/$MgAl_2O_4$-cop, respectively. The Ir 4f signal, the most intense for iridium, overlaps with one Al 2p (plasmon) signal coming from the support ($MgAl_2O_4$). However, it is possible to decompose the signal and to separate the components. For the Ir(0.5)/$MgAl_2O_4$-citr catalyst (Figure 17), the presence of the Ir $4f_{7/2}$ and Ir $4f_{5/2}$ doublet, placed at 60.7 and 63.4 eV of binding energy, respectively, indicates the existence of zerovalent Ir [33] in this reduced catalyst. For the Ir(0.5)/$MgAl_2O_4$-cop catalyst, the Ir $4f_{7/2}$ and Ir $4f_{5/2}$ doublet, located at 61.0 and 63.0 eV of binding energy, respectively (Figure 18), is also attributed to zerovalent Ir.

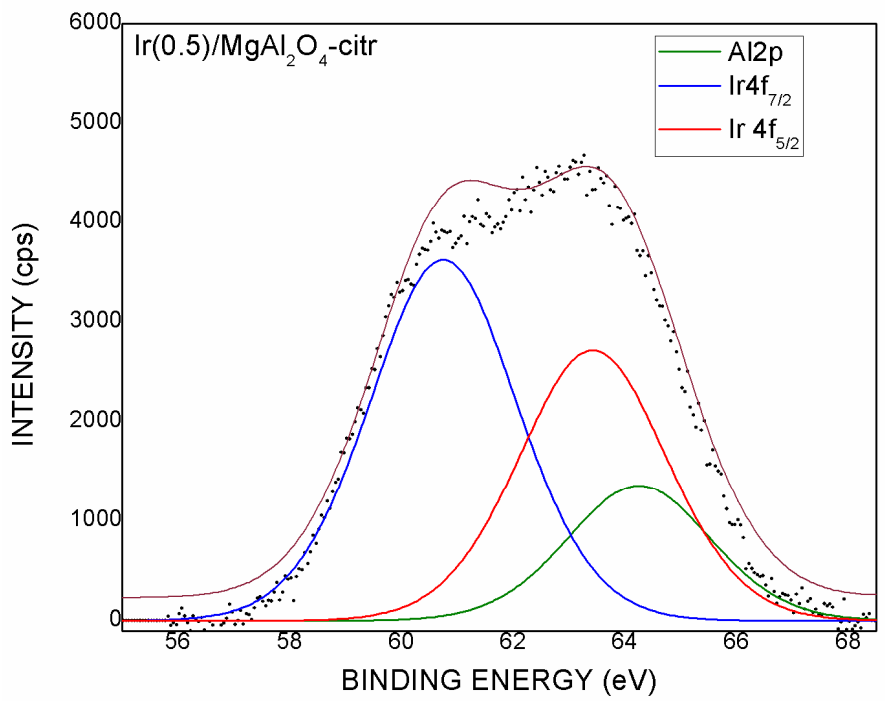

Figure 17. XPS of Ir 4f signals for Ir(0.5)/$MgAl_2O_4$-citr.

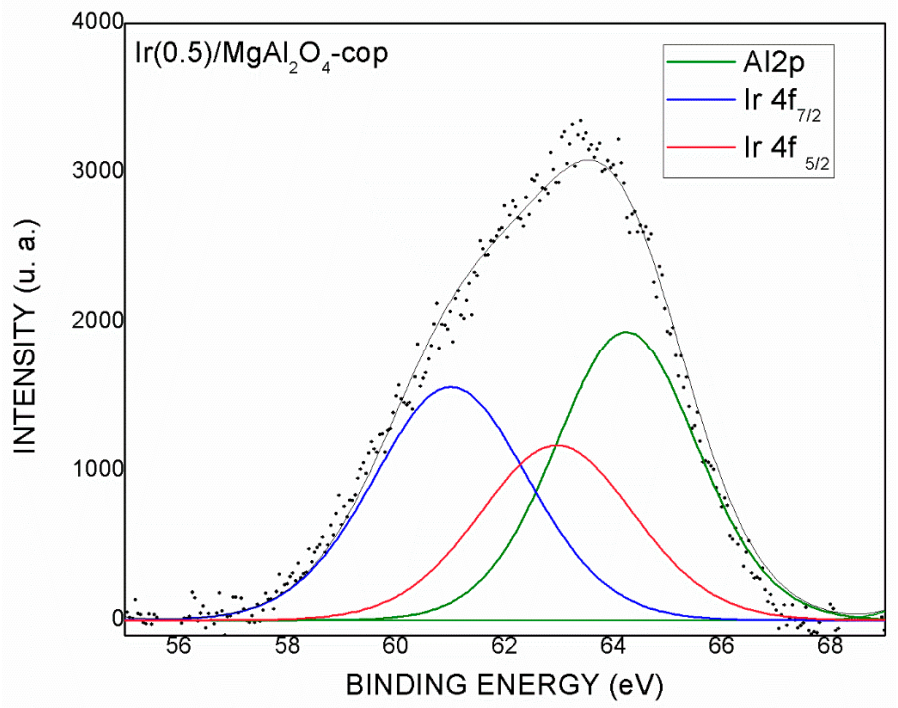

Figure 18. XPS of Ir 4f signals for Ir(0.5)/$MgAl_2O_4$-cop.

Figures 19 and 20 show XPS spectra of Ir $4f_{7/2}$ and Ir $4f_{5/2}$ signals for both reduced bimetallic catalysts, Ir(0.5)Sn(0.7)/$MgAl_2O_4$-citr and Ir(0.5)Sn(0.7)/$MgAl_2O_4$-cop, respectively. For both catalysts, the Ir $4f_{7/2}$ and $4f_{5/2}$ doublets appear at 60.8 and 63.3 eV, and at 61.0 and 62.9 eV of binding energy, respectively, which also indicates the existence of zerovalent Ir in both catalysts.

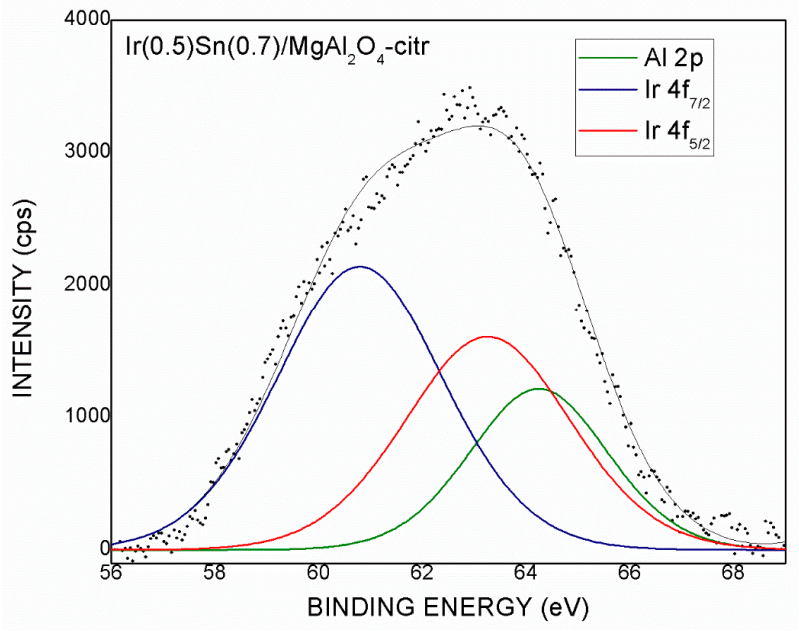

Figure 19. XPS of Ir 4f signals for Ir(0.5)Sn(0.7)/$MgAl_2O_4$-citr.

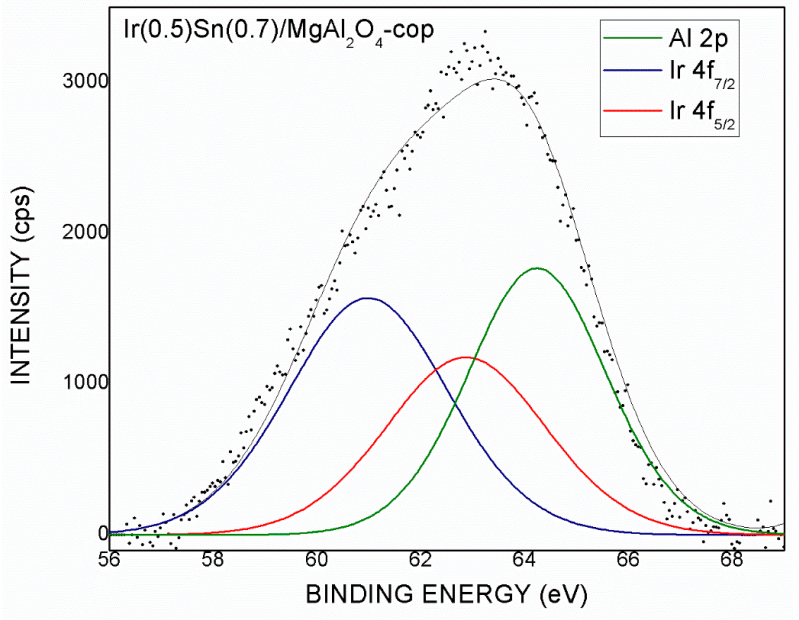

Figure 20. XPS of Ir 4f signals for Ir(0.5)Sn(0.7)/$MgAl_2O_4$-cop.

With respect to the surface characterization of the Sn species, Figure 21 shows the Sn $3d_{5/2}$ signal for the Ir(0.5)Sn(0.7)/$MgAl_2O_4$-citr catalyst. This signal was decomposed into two peaks located at 484.9 eV and 487.0 eV. The first peak corresponds to zerovalent Sn, while the second one can be attributed to tin oxides [33]. For the other bimetallic catalyst Ir(0.5)Sn(0.7)/$MgAl_2O_4$-cop, Figure 22 also shows two peaks derived from the decomposition of the Sn $3d_{5/2}$ signal, which correspond to zerovalent Sn (484.7 eV) and tin oxides (486.8 eV). Both catalysts show a high proportion of zerovalent tin, with 54% for the first bimetallic catalyst and 49% for the second one. Taking into account that monometallic Sn catalysts supported on $MgAl_2O_4$ showed only tin oxides [5], the presence of zerovalent tin in both bimetallic catalysts would be due to the presence of electronic interactions between iridium and tin with probable Ir-Sn alloy formation during the reduction treatment. These XPS results are in agreement with the phenomenon observed in TPR experiments, where strong interactions between Ir and Sn metals in both catalysts were observed. Thus, it

can be inferred that in bimetallic catalysts, a large part of the tin is located In Ir-Sn bimetallic clusters, where it is reduced during the reductive treatment, while the other part is more in interaction with the support, where it remains oxidized.

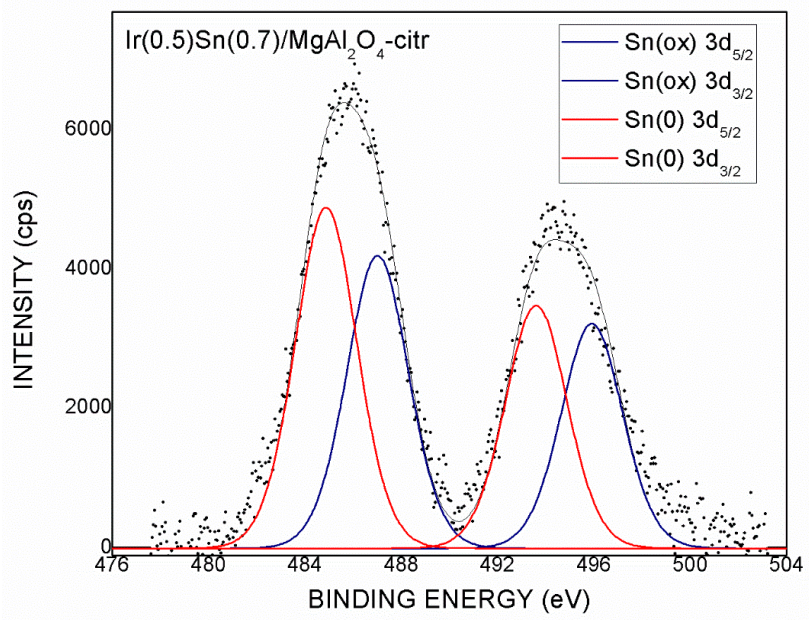

Figure 21. XPS of Sn 3d signals for Ir(0.5)Sn(0.7)/$MgAl_2O_4$-citr.

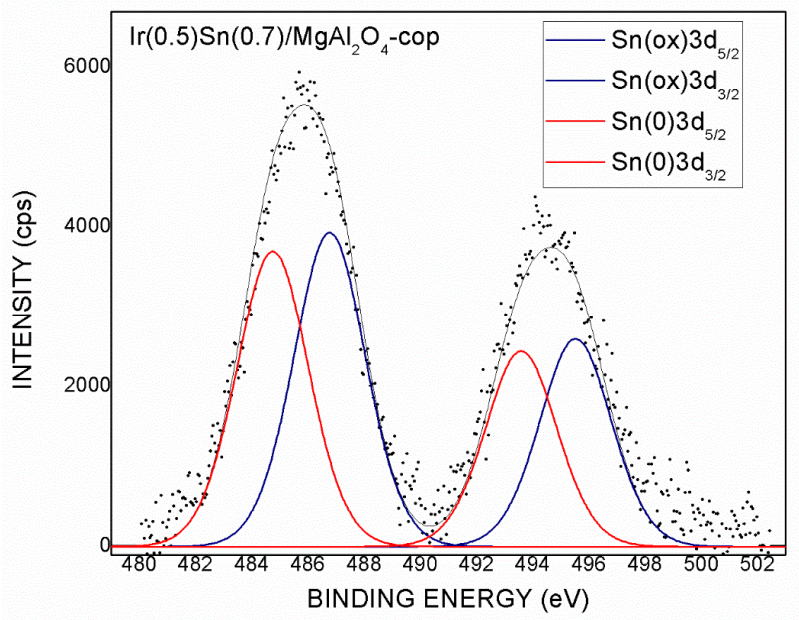

Figure 22. XPS of Sn 3d signals for Ir(0.5)Sn(0.7)/$MgAl_2O_4$-cop.

Similar results of Ir-Sn alloy formation or important electronic modifications of Sn on Ir were observed by different authors. In this sense, Gallo et al. studied IrSn catalysts supported on SiO_2 [12] and, by using XANES experiments, found a notable Sn → Ir donation, suggesting at least a very important electronic effect in the metallic particles, with alloy formation, and this effect leads to good catalytic properties in the dehydrogenation reaction of light paraffins. Furthermore, Lazar et al. [13], by using Mossbauer spectroscopy, detected oxidized and zerovalent tin on IrSn catalysts supported on alumina, and found mainly iridium–tin alloys on similar bimetallic catalysts supported on silica. Sommerville and Shapley [16] detected the formation of bimetallic Ir-Sn particles via the EDX analysis

of IrSn/zeolite catalysts. Finally, Zhang et al. [17] confirmed using XANES and EXAFS results that the introduction of Sn atoms promotes the transfer of electrons from Sn atoms to Ir atoms, forming electron-rich $Ir^{\delta+}$ species. Another factor to take into account is based on studies about the formation of bimetallic complexes containing Ir and Sn during the preparation of the catalysts. In this sense, Maity et al. [34] synthesized Ir-Sn bimetallic complexes by inserting stannous chloride (SnCl2) into an Ir-Cl bond, which could facilitate the intermetallic interaction.

4. Discussion

Two magnesium aluminate synthesis methods were used to develop the catalytic supports, the coprecipitation and the citrate–nitrate combustion methods. Both synthesis techniques led to the formation of $MgAl_2O_4$ with high specific surfaces, the former being an essentially mesoporous material and the latter with a mixture of micro- and mesoporosity. Taking into account that catalytic supports for light paraffin dehydrogenation must have low acidity to inhibit secondary reactions such as paraffin cracking, characterization by FTIR of the adsorbed pyridine showed a very low acidity of both materials. These properties make them very suitable as supports for dehydrogenation catalysts. Another property that good catalytic supports must have is to promote a good metal–support interaction that leads to a very high dispersion of the metallic phase. In this sense, TEM results of the Ir and IrSn catalysts supported on both $MgAl_2O_4$ proved that subnanometer atomic clusters are formed on the surface, which confirms the good interaction between the metals and both supports, giving rise to ultradisperse mono- and bimetallic catalysts.

The catalytic evaluations of the monometallic Ir catalysts supported on both supports determined that Ir supported on $MgAl_2O_4$ is a strongly hydrogenolytic metal and therefore non-selective in the n-butane dehydrogenation reaction towards the different C4 olefins. Compared with Pt supported on $MgAl_2O_4$, Ir is more strongly hydrogenolytic [12,26]. The C-C bond-breaking capacity of Ir was confirmed through a widely used test reaction, the cyclopentane hydrogenolysis. This reaction, which is sensitive to the structure just like n-butane hydrogenolysis, requires an ensemble of metal atoms to be carried out. The small Ir ensembles adsorb the cyclopentane molecule, producing C-C bond breaks in all its parts, giving mainly methane and other light gases, while the selectivity to n-pentane is practically negligible in both monometallic Ir catalysts.

For the bimetallic IrSn/ $MgAl_2O_4$ catalysts, the promoter role of Sn strongly decreases the hydrogenolytic capacity of the active metal, improving not only the n-butane conversion but also the selectivity to butenes up to 80–90%. Additionally, the activity falls along the reaction time are diminished with the consequent increase of the catalytic stability. This has a favorable impact on the yield towards butenes, being slightly higher in the IrSn catalysts supported on $MgAl_2O_4$-cop than those supported on $MgAl_2O_4$-citr. Furthermore, the highest yields were achieved with the higher Sn content. In this sense, the decreasing order of initial butene yields for mono- and bimetallic catalysts follows the following sequence:

$$\begin{gathered}Ir(0.5)Sn(0.9)/MgAl_2O_4\text{-cop} > Ir(0.5)Sn(0.7)/MgAl_2O_4\text{-cop} > Ir(0.5)Sn(0.9)/MgAl_2O_4\text{-citr} > \\ Ir(0.5)Sn(0.5)/MgAl_2O_4\text{-cop} \cong Ir(0.5)Sn(0.7)/MgAl_2O_4\text{-citr} > Ir(0.5)Sn(0.5)/MgAl_2O_4\text{-citr} >> \\ Ir(0.5)/MgAl_2O_4\text{-cop} \cong Ir(0.5)/MgAl_2O_4\text{-citr}\end{gathered}$$

The small differences in the olefin yields in favor of the bimetallic catalysts supported on $MgAl_2O_4$-cop with respect to those supported on $MgAl_2O_4$-citr could be related to the sizes of the atomic clusters, since if we compare the average diameters, the catalysts supported on $MgAl_2O_4$-cop not only have smaller sizes but also a narrower distribution than those supported on $MgAl_2O_4$-citr.

This work confirms the existence of strong interactions between Ir and Sn in both types of bimetallic catalysts through the results of TPR experiments and XPS analysis. TPR results of the different bimetallic catalysts show a broadening of the main reduction area, which indicates a co-reduction phenomenon of Ir and Sn species with the probable formation of alloys. This phenomenon is more pronounced for bimetallic catalysts with

the highest Sn loadings (0.9%) that present a shift to lower reduction temperatures of the main reduction peak. Likewise, the drastic drop in the reaction rate values for the cyclopentane hydrogenolysis (structure-sensitive reaction) of bimetallic catalysts with respect to the corresponding monometallic Ir catalysts also indicates an important effect of tin on the iridium sites, which is not only geometric (intercalation/dilution) but also electronic. Finally, the XPS results of reduced bimetallic catalysts show that Sn is present in two oxidation states, half in the zerovalent state, probably alloyed with Ir(0), and the other half as ionic tin, probably close to the Ir–support interface. Similar XPS results were found for structured PtSn/$MgAl_2O_4$-coated supports, though the ratio between the zerovalent tin and oxidized tin was much lower [18,35]. The high degree of reduction of the Sn promoter to the zerovalent state in the bimetallic catalysts contrasts with the null reduction in the catalysts without the presence of Ir, which demonstrates the presence of strong electronic interactions between Ir and the promoter.

As previously stated, the non-oxidative direct dehydrogenation process of light paraffins such as n-butane is simultaneously constituted by desirable reactions such as the dehydrogenation of paraffins to olefins, which are insensitive to the structure, and undesirable reactions such as hydrogenolysis, which are sensitive to structure. To correlate the catalytic performances of the different catalysts with their surface characteristics, on the one hand, we can say that the Sn promoter added to Ir produces geometrical effects, inhibiting the formation of adjacent-atom aggregates or ensembles, which are responsible for the C-C bonds' rupture, drastically decreasing the hydrogenolysis reactions of n-butane leading to light gases. On the other hand, this dilution effect does not justify the important increase in the dehydrogenation selectivity to the different butenes. Taking into account the insensitive character of the dehydrogenation reaction, the presence of strong interactions that modify the electronic density of the Ir sites due to Sn would be responsible for the notable catalytic behavior of bimetallic IrSn catalysts supported on both $MgAl_2O_4$ supports prepared using different techniques. Regarding the improvement in catalytic stability, this is due to the fact that the metallic interactions between the active metal and the promoter would decrease the coke-formation reactions, which are responsible for the activity loss in the monometallic Ir catalysts.

5. Conclusions

The coprecipitation and citrate–nitrate combustion methods used to synthesize $MgAl_2O_4$ lead to materials with very low acidity and high surface areas, thus favoring both the inhibition of undesirable reactions and the metallic dispersion when used as supports for metallic catalysts.

The microscopic characterization of the Ir and IrSn catalysts supported on both types of $MgAl_2O_4$ revealed that the sizes of the atomic clusters present on the catalytic surfaces are subnanometer, which would confirm the good metal–support interaction and the very high dispersion in these mono- and bimetallic catalysts.

The addition of Sn to Ir produces an increase in the conversion of n-butane and a drastic decrease in hydrogenolysis, bringing the dehydrogenating selectivity towards butenes to very high values. The best catalytic behaviors are achieved with bimetallic catalysts with higher Sn contents and supported on $MgAl_2O_4$ prepared by coprecipitation. In this sense, the best catalyst is Ir(0.5)Sn(0.9)/ $MgAl_2O_4$-cop.

The addition of Sn to Ir produces geometric and electronic effects in the metallic phase of bimetallic catalysts. The combination of these effects would be the cause of the notable catalytic behavior of the bimetallic IrSn catalysts supported on $MgAl_2O_4$ prepared using the two techniques.

Author Contributions: Conceptualization, S.d.M., C.E., F.E., S.B.; methodology, S.d.M., V.B., C.E., F.E., S.B.; investigation, J.F., V.B., C.E.; resources, F.E., S.B.; data curation, J.F.; writing—original draft, S.d.M., V.B., S.B.; writing–review & editing, S.d.M., C.E., F.E., S.B.; visualization, V.B.; supervision, S.d.M., S.B.; project administration, F.E., S.B.; funding acquisition, F.E., S.B. All authors have read and agreed to the published version of the manuscript.

Funding: This research was funded by CNRS as part of the international research project OLECAT. This work pertains to the French government program "Investissements d'Avenir" (EUR INTREE, reference ANR-18-EURE-0010). This research was also funded by Universidad Nacional del Litoral (CAI+D program, PIC: 50420150100050LI) and CONICET (PIP: 11220170100417CO) (Argentina).

Data Availability Statement: The original contributions presented in the study are included in the article, further inquiries can be directed to the corresponding author/s.

Acknowledgments: The authors thank the collaboration project between the INCAPE (Santa Fe, Argentina) and IC2MP laboratories (Poitiers, France) as part of the international research project OLECAT.

Conflicts of Interest: The authors declare no conflict of interest.

References

1. Nawaz, Z. Light alkane dehydrogenation to light olefin technologies: A comprehensive review. *Rev. Chem. Eng.* **2015**, *31*, 413–436. [CrossRef]
2. Bhasin, M.M.; McCain, J.H.; Vora, B.V.; Imai, T.; Pujadó, P.R. Dehydrogenation and oxydehydrogenation of paraffins to olefins. *Appl. Catal. A* **2001**, *221*, 397–419. [CrossRef]
3. Sattler, J.J.H.B.; Ruiz-Martinez, J.; Santillan-Jimenez, E.; Weckhuysen, B.M. Catalytic Dehydrogenation of Light Alkanes on Metals Metal Oxides. *Chem. Rev.* **2014**, *114*, 10613–10653. [CrossRef]
4. Armendáriz, H.; Guzmán, A.; Toledo, J.A.; Llanos, M.E.; Vázquez, A.; Aguilar-Rıos, G. Isopentane dehydrogenation on Pt-Sn catalysts supported on Al-Mg-O mixed oxides: Effect of Al/Mg atomic ratio. *Appl. Catal. A* **2001**, *211*, 69–80. [CrossRef]
5. Bocanegra, S.A.; Guerrero-Ruiz, A.; de Miguel, S.R.; Scelza, O.A. Performance of PtSn catalysts supported on MAl_2O_4 (M: Mg or Zn) in n-butane dehydrogenation: Characterization of the metallic phase. *Appl. Catal. A* **2004**, *277*, 11–22. [CrossRef]
6. Sun, P.; Siddiqi, G.; Vining, W.C.; Chi, M.; Bell, A.T. Novel Pt/Mg(In)(Al)O catalysts for ethane and propane dehydrogenation. *J. Catal.* **2011**, *282*, 165–174. [CrossRef]
7. Bocanegra, S.A.; Castro, A.A.; Scelza, O.A.; de Miguel, S.R. Characterization and catalytic behavior in the n-butane dehydrogenation of trimetallic InPtSn/$MgAl_2O_4$ catalysts. *Appl. Catal. A* **2007**, *333*, 49–56. [CrossRef]
8. Fang, S.; Bi, K.; Zhang, Q.; Sun, Y.; Huang, H.; Ma, L.; Wang, C. Performance of Ethane Dehydrogenation over PtSn Loaded onto a Calcined Mg(Al)O LDH with Three Mg:Al Molar Ratios Using a Novel Method. *Catalysts* **2018**, *8*, 296–310. [CrossRef]
9. Ballarini, A.D.; Zgolicz, P.; Vilella, I.M.J.; de Miguel, S.R.; Castro, A.A.; Scelza, O.A. n-Butane dehydrogenation on Pt, PtSn and PtGe supported on γ-Al_2O_3 deposited on spheres of α-Al_2O_3 by washcoating. *Appl. Catal. A* **2010**, *381*, 83–91. [CrossRef]
10. Homs, N.; Llorca, J.; Riera, M.; Jolis, J.; Fierro, J.L.G.; Sales, J.; Ramírez de la Piscina, P. Silica-supported PtSn alloy doped with Ga, In or, Tl: Characterization and catalytic behaviour in n-hexane dehydrogenation. *J. Mol. Catal. A* **2003**, *200*, 251–259. [CrossRef]
11. Maina, S.C.P.; Ballarini, A.D.; Vilella, I.M.J.I.; de Miguel, S.R. Study of the performance and stability in the dry reforming of methane of doped alumina supported iridium catalysts. *Catal. Today* **2020**, *344*, 129–142. [CrossRef]
12. Gallo, A.; Psaro, R.; Guidotti, M.; Dal Santo, V.; Della Pergola, R.; Masih, D.; Izumi, Y. Cluster-derived Ir–Sn/SiO_2 catalysts for the catalytic dehydrogenation of propane: A spectroscopic study. *Dalton Trans.* **2013**, *42*, 12714–12724. [CrossRef]
13. Lazar, K.; Bussiere, P.; Guenin, M.; Frety, R. Stabilization of Tin in bimetallic Iridium-Tin systems supported on alumina and silica. Mossbauer spectroscopy and catalytic activity. *Appl. Catal.* **1988**, *38*, 19–40. [CrossRef]
14. Guidotti, M.; Dal Santo, V.; Gallo, A.; Gianotti, E.; Peli, G.; Psaro, R.; Sordelli, L. Catalytic dehydrogenation of propane over cluster-derived Ir–Sn/SiO2-Catalysts. *Catal. Lett.* **2006**, *112*, 89–95. [CrossRef]
15. Chen, X.; Qin, X.; Jiao, Y.; Peng, M.; Diao, J.; Ren, P.; Li, C.; Xiao, D.; Wen, X.; Jiang, Z.; et al. Structure-dependence and metal-dependence on atomically dispersed Ir catalysts for efficient n-butane dehydrogenation. *Nat. Commun.* **2023**, *14*, 2588–2599. [CrossRef]
16. Sommerville, D.M.; Shapley, J.R. Zeolite-NaY-supported Ir/Sn catalysts derived from single- and dual-source organometallic precursors. Preparation and characterization of highly selective dehydrogenation catalysts. *Catal. Lett.* **1998**, *52*, 123–129. [CrossRef]
17. Zhang, Y.; Shi, S.; Wang, Z.; Lan, H.; Liu, L.; Sun, Q.; Guo, G.; He, X.; Ji, H. Propane dehydrogenation on Ir single-atom catalyst modified by atomically dispersed Sn promoters in silicalite-1 zeolite. *AIChE J.* 2024, *in press*. [CrossRef]
18. de Miguel, S.R.; Vilella, I.M.J.; Zgolicz, P.; Bocanegra, S.A. Bimetallic catalysts supported on novel spherical $MgAl_2O_4$-coated supports for dehydrogenation processes. *Appl. Catal. A* **2018**, *567*, 36–44. [CrossRef]
19. Li, J.; Ikegami, T.; Lee, J.; Mori, T.; Yajima, Y. Synthesis of Mg–Al spinel powder via precipitation using ammonium bicarbonate as the precipitant. *J. Eur. Ceram. Soc.* **2001**, *21*, 139–148. [CrossRef]
20. Wajler, A.; Tomaszewski, H.; Drożdż-Cieśla, E.; Węglarz, H.; Kaszkur, Z. Study of magnesium aluminate spinel formation from carbonate precursors. *J. Eur. Ceram. Soc.* **2008**, *28*, 2495–2500. [CrossRef]
21. Cordoba, M.; Betti, C.; Martínez Bovier, L.; García, L.; Coloma-Pascual, F.; Ramírez, A.; Quiroga, M.; Lederhos, C. Role of the support and chloride during the purification of 1-pentene in alkyne/alkene streams over Pd catalysts. *J. Chem. Technol. Biotechnol.* **2021**, *96*, 2283–2297. [CrossRef]

22. Guisnet, M.; Magnoux, P. Organic Chemistry of Coke Formation. *Appl. Catal. A* **2001**, *212*, 83–96. [CrossRef]
23. Cheng, Z.X.; Ponec, V. Selective Isomerization of Butene to Isobutene. *J. Catal.* **1994**, *148*, 607–616. [CrossRef]
24. Flaherty, D.W.; Hibbitts, D.D.; Iglesia, E. Metal-catalyzed C-C bond cleavage in alkanes: Effects of methyl substitution on transition-state structures and stability. *J. Am. Chem. Soc.* **2014**, *136*, 9664–9676. [CrossRef]
25. Boudart, M.; Djéga-Mariadassou, G. *Kinetics of Heterogeneous Catalytic Reactions*; Princeton University Press: Princeton, NJ, USA, 2014.
26. Zhang, X.; Lu, Y.; Kovarik, L.; Dasari, P.; Nagaki, D.; Karim, A.M. Structure sensitivity of n-butane hydrogenolysis on supported Ir Catalysts. *J. Catal.* **2021**, *394*, 376–386. [CrossRef]
27. Foger, K.; Anderson, J.R. Hydrocarbon reactions on supported iridium catalysts. *J. Catal.* **1979**, *59*, 325–339. [CrossRef]
28. Walter, C.G.; Coq, B.; Figueras, F.; Boulet, M. Competitive reaction of methylcyclohexane and n-hexane over alumina-supported platinum, iridium and ruthenium catalysts. *Appl. Catal. A* **1995**, *133*, 95–102. [CrossRef]
29. Locatelli, F.; Uzio, D.; Niccolai, G.; Basset, J.; Candy, J.P. Hydrogenolysis of 1,4-dimethylcyclohexane on silica supported iridium catalyst: Influence of time on stream on activity and selectivity. *Catal. Commun.* **2003**, *4*, 189–194. [CrossRef]
30. Deng, C.; Duan, X.; Zhou, J.; Zhou, X.; Yuan, W.; Scott, S.L. Ir-Re alloy as a highly active catalyst for the hydrogenolysis of glycerol to 1,3-propanediol. *Catal. Sci. Technol.* **2015**, *5*, 1540–1547. [CrossRef]
31. Taketoshi, A.; Haruta, M. Size- and Structure-specificity in Catalysis by Gold Clusters. *Chem. Lett.* **2014**, *43*, 380–387. [CrossRef]
32. Ishida, T.; Murayama, T.; Taketoshi, A.; Haruta, M. Importance of Size and Contact Structure of Gold Nanoparticles for the Genesis of Unique Catalytic Processes. *Chem. Rev.* **2020**, *120*, 464–525. [CrossRef] [PubMed]
33. Moulder, J.F.; Stickle, W.F.; Sobol, P.E.; Bomben, K.D. *Handbook of X-ray Photoelectron Spectroscopy*; Perkin-Elmer Corporation: Waltham, MA, USA, 1992.
34. Maity, A.K.; Bhattacharjee, M.; Roy, S. $SnCl_2$ insertion into Ir-Cl and Rh-Cl bonds: Synthesis, characterization and catalytic activity of three-legged piano-stool trichlorostannyl iridium and rhodium complexes. *J. Organomet. Chem.* **2014**, *768*, 42–49. [CrossRef]
35. Ballarini, A.; Zgolicz, P.; de Miguel, S.; Bocanegra, S. Stability studies of PtSn structured catalysts supported on thin layers of MAl_2O_4 (M: Mg, or Zn) for paraffins dehydrogenation reactions. *Can. J. Chem. Eng.* **2023**, *101*, 431–443. [CrossRef]